Environ. Water Eng., 2025, 11(4), 486-498 https://doi.org/10.22034/ewe.2025.515336.2014

Environment and Water Engineering

Homepage: www.jewe.ir

ISSN: 2476-3683

Simulation of flow pattern in alluvial channel and 60-degree lateral intake through the numerical FLOW-3D model

Amir Moradinejad[1]✉, Amir Hamzeh Haghiabi[2], Mojtaba Saneie[3], and Hojatallah Yonesi[2]

[1]Soil Conservation and Watershed Management Research Department, Markazi Agricultural and Natural Resources Research and Education Center, AREEO, Arak, Iran
[2]Water Engineering Department, Faculty of Agriculture, Lorestan University, Khorramabad, Iran
[3]Soil Conservation and Watershed Management Institute (SCWMRI), Tehran, Iran

ARTICLE INFO

Paper Type: Research Paper

Received: 06 April 2025
Revised: 23 April 2025
Accepted: 17 May 2025
Published: 01 June 2025

Keywords
Flow3D
Intake
Sediment Control
Skimming Wall
Spur Dike

Corresponding author:
A. Moradinejad
✉ amir_24619@yahoo.com

ABSTRACT

To reduce sediment entering the intake, a set of structures can be used to control sediment entry into the intake. In this study, a skimming wall structure has been used for the first time to control sediment entry into the intake. Using the three-dimensional numerical model FLOW3D, the flow field around the lateral intake located in the straight path has been numerically solved. Experiments were conducted on the flume in the laboratory, and the results of the numerical model were compared with those of the laboratory model. The results showed that by installing a skimming wall in front of the intake, the flow separation width near the bed with more sediment decreases, and increases at the level with less sediment. Inside the intake, the surface flow lines tend to the right wall, and the bottom flow lines tend to the left wall of the intake. By adding a spur dike structure at an angle of 60 degrees and at a distance of 2b from the center of the intake mouth in the main channel, the resulting velocity in the main channel is 1.5 times the two cases without a spur dike and with a skimming wall. The presence of the spur dike has increased the longitudinal velocity in the layer near the bottom by 2.25 times and the transverse velocity in the surface layer by 1.33 times compared to the case without the spur dike.

Highlights

- No prior numerical modeling studies on skimming walls.
- Skimming wall and spur dike boosts sediment control and flow guidance.
- Spur dike raises the bottom-layer longitudinal velocity by 2.25 times.
- Spur dike elevates surface-layer transverse velocity by 1.33 times.

Citing:
Moradinejad, A., Haghiabi, A., Saneie, M., & Yonesi, H. (2025). Simulation of flow pattern in alluvial channel and 60-degree lateral intake through the FLOW-3D numerical model. *Environment and Water Engineering*, *11*(4), 486-498. https://doi.org/10.22034/ewe.2025.515336.2014

1. Introduction

Water intake from rivers is one of the most critical topics in hydraulic engineering. A common challenge associated with most intakes is the accumulation of sediment at their entrances. Failure to control sediment entering the intakes results in its transfer into irrigation canals and facilities, leading to numerous problems caused by sediment transport or deposition in various sections. With advancements in computational systems and the complexities of water flow and sediment transport in laboratory models, numerical simulations have become a highly effective and valuable tool for investigating such hydraulic phenomena (Amini et al. 2017). FLOW-3D software is capable of numerically simulating flow and sediment patterns around various hydraulic structures. Neary et al. (1999) developed and validated a three-dimensional **k-ω** model for dividing flows in an open-channel T-diversion. A parametric study was conducted on discharge ratios, aspect ratios, and main channel bed roughness distribution. However, the absence of three-dimensional velocity measurements limited a more detailed assessment of their calculations. More recently, Li and Zeng

(2009) developed a three-dimensional model with Spalart-Allmaras turbulence closure to investigate flows in channel diversions with varying width ratios and different vegetation densities in the branch channel. Their numerical results accurately predicted the trend of increasing flow in the branch channel with an increase in branch channel width and/or a decrease in vegetation density. Aghaei et al. (2015) numerically simulated turbulent flow and local scour around a spur dike by solving the three-dimensional Navier-Stokes equations along with sediment transport equations using the FLOW-3D numerical model. In their study, two turbulence models, **k-ε** and RNG (Renormalized Group), were compared for their ability to predict maximum scour depth under laboratory conditions. The RNG turbulence model produced more accurate and reliable results. Zhou et al. (2009) developed a relatively new 3D LES-RANS hybrid model to simulate T-deviation flows in open channels. Their model was validated with a classic case of a fully developed open channel turbulent flow. This model was then used to simulate the flow in a T-deviation in an open channel. Comparison between numerical results and accurate velocity measurements showed that the hybrid model accurately reproduces the mean flow characteristics, such as velocity profiles and mean flow patterns. With the turbulence resolved, further work can be done on the turbulence characteristics of T-deviation flows. Assuming nearly uniform velocities, Hsu et al. (2002) presented a depth-discharge relationship and energy-loss coefficient for subcritical, equal-width, right-angled dividing flows over a horizontal bed in a narrow aspect ratio channel. Sarvari et al. (2015) evaluated the use of FLOW-3D to predict morphological changes at river confluences. Comparisons between numerical and experimental results showed that this model could simulate the maximum height of sedimentation at the intersection of sub-canals with an average error of about 6.3%. However, it had an average error of approximately 26% when simulating erosion depth on the right bank of the main canal under various flow rate conditions. Using FLOW-3D, Pour Bahman (2015) simulated sediment flow entering intake structures at pumping stations in Darehshahr (Cham Zhab and Armo pumping stations) located on the outer bend of the Seymareh River. The study examined the effects of intake discharge on separation zone dimensions, sediment volume, and inflow rate .Using FLOW-3D software, Rahmani Firoozjany et al. (2015) showed that the numerical model was acceptably accurate. Moreover, their comparison of numerical simulations for intake angles of 30, 60, and 90 degrees revealed that a 60-degree angle to the main canal resulted in the most efficient dewatering compared to the other two angles.

Acharya et al. (2013) performed three-dimensional numerical investigations on turbulent flow models around a series of blade spur dikes aligned in a straight line with fixed or moving beds using FLOW-3D. Ettema and Muste (2004) examined the effects of spur dike length on the rotational area behind the spur dike, considering scale effects, using FLOW-3D. To investigate the impact of sedimentary internal friction angle on scour holes, Amirarsalani (2008) conducted a three-dimensional simulation of scouring downstream of a free-falling jet using FLOW-3D's **k-ε** model. Shahrokhi (2008) developed a numerical model of flow patterns around a spur dike using FLOW-3D and evaluated the impact of different turbulence models on the length of the flow separation region behind the spur dike. The results indicated that the Large Eddy Simulation (LES) turbulence model was the most effective for predicting the separation region. Shamlou and Ja'ffari (2008) used FLOW-3D and the **k-ε** turbulence model to investigate the effect of floor roughness on changes in flow velocity and pressure fields around a cylindrical base in a rectangular channel. Ardeshir and Sanei (2014) studied the effect of spur dike length and location on intake flow using a permeable spur dike in lateral intakes. Their results suggested that increasing the spur dike length resulted in higher flow rates. For intake percentages of 5, 11, and 20%, moving the spur dike further downstream from the intake entrance increased intake discharge percentages.

Abbaspour et al. (2009) evaluated a two-dimensional numerical simulation of a hydraulic jump on a wavy bed using standard k-ε and RNG k-ε models. The free surface was determined using the VOF method. The results showed that the turbulent k-ε model and the VOF method are suitable for predicting the water level in a jump on a wavy bed, and the relative error of the predicted water level profiles and the measured value is in the range of 1 to 8.6%. The study of the axial velocity profiles at different sections of the jump showed that the velocity profiles in different experiments were similar and there was a good agreement between the modeled and measured results. The effects of waves (t, s) on the basic characteristics of the jump, such as the free surface position, velocity, and shear stress distribution, were studied for different ranges of Froude number.

Moradinejad et al. (2017) experimentally investigated the effect of skimming walls on controlling sediment entry at lateral intakes. Their results showed that combining a skimming wall with a spur dike reduced sediment entry by 81%, 78.5%, and 76% on average for walls with angles of 10, 14, and 18 degrees, respectively. This combination was more effective than using a skimming wall alone, reducing sediment entry by about 15%. Moradinejad et al. (2019) indicated that using a skimming wall, either alone or combined with a spur dike, allowed directing the thalweg toward the intake port. Additionally, the skimming wall created a trench toward the intake, increasing impoundment efficiency by 81% when combined with a spur dike and up to 66% when used alone. Karimi Sarmeydani et al. (2024) concluded that GEP is relatively superior to support vector machine (SVM) and FLOW-3D. Amini et al. (2024) revealed significant discrepancies between estimated and measured scour depths in a complex pier. Ahmed et al. (2025) investigated scour at box culverts with inlet blockages of 0%, 15%, and 30%. The analysis revealed that predictions from numerical models corresponded closely with experimental outcomes, although the scour depths calculated by the models were generally lower than those observed under both steady and unsteady flow conditions.

Few studies have been conducted so far on the combination of a new structure (Skimming wall) and a breakwater in a channel, and their effect on the velocity and characteristics of the flow. The presence of many parameters in the sedimentation pattern in the water intake from the channels has complicated the theory of flow at the intersection of the channels. Studying the bifurcation flow and understanding the

behavior of the flow in the areas of separation into two flows requires studying the flow pattern and dynamics. Understanding the flow pattern in the flow bifurcation areas can be a key to predicting sedimentary processes. This research aimed to determine the effect of two structures on the flow behavior and velocity in two dimensions around the lateral intake so that the maximum flow with the least amount of sediment enters the intake.

2. Materials and Methods

2.1 The Laboratory Flume

The experiments were conducted in the hydraulic laboratory using a 12 m long flume with a width of 5.1 m and a height of 9.0 m (Fig. 1). The flume featured a water and sediment circulation system. Dewatering was achieved through a lateral canal that was 0.6 m wide, 2.5 m long, and positioned at a 60-degree angle to the flow direction in the main channel. Rectangular and triangular sharp-edged spillways were used to measure the flow in the main canal and intake. A two-dimensional electromagnetic speedometer with an accuracy of ±0.001 m/s was employed to measure the velocity and direction of the flow. An altimeter (Point Gage) and Profiler with an accuracy of ±0.1 mm were used to measure the water surface profile. The skimming wall structure consisted of two branches. The first branch was 75 cm long and 25 cm high, with one side connected to the intake bank and the other to the second branch. The second branch, parallel to the bank, was 112 cm long and 25 cm high, extending in the direction of the flow. The height above the bed was one-third of the flow depth. Based on Barkdoll's research, the ratio of the branches' lengths was set at $L_2/L_1=1.5$. To direct the flow, a spur dike with an angle of 60 degrees, a length of 0.25B, and positioned at a distance of 2b from the intake center was used on the wall opposite the intake. The sediments used in these experiments were sands with a diameter of 1 mm, a density of 2.65, a standard deviation of 1.47, and a uniformity coefficient of 2.2.

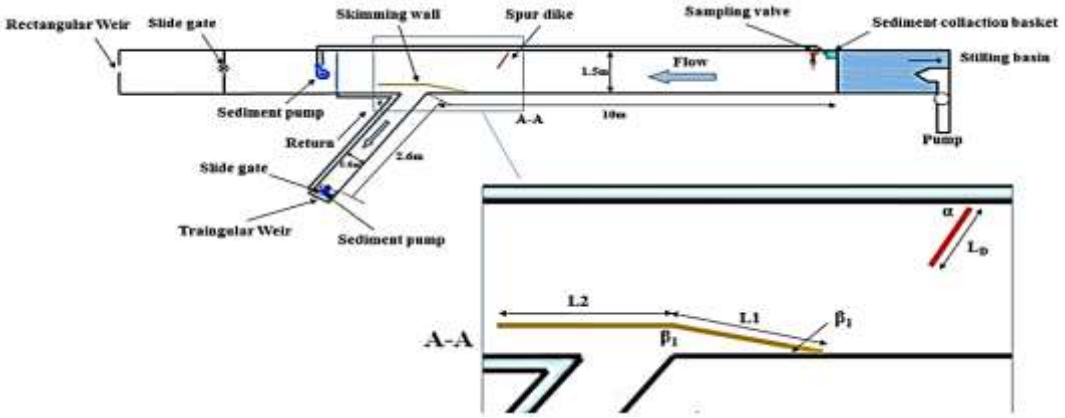

Fig. 1 A schematic of flume, spur dike, skimming wall, and water circulation system and sediment (Moradinejad et al. 2019)

2.2 FLOW-3D

The model is able to do one, two, and three-dimensional analysis of the flow field. The basic equations used in this model are the Navier-Stokes equations. It consists of five turbulence models: Prandtl mixing length, one equation, Turbulent energy model, Two equation k-ε model (RNG k-ε), Renormalized group model, and Large eddy simulation model. In this software, the flow standard equations, like Navier-Stokes and continuity equations, are numerically solved for the entire computing space. Continuity equation at three-dimensional Cartesian coordinates given as Eq. 1 (Ghasemzadeh, 2013).

$$v_f \frac{\partial \rho}{\partial t} + \frac{\partial}{\partial x}(uA_x) + \frac{\partial}{\partial x}(vA_y) + \frac{\partial}{\partial x}(wA_z) = \frac{PSOR}{\rho} \quad (1)$$

Where *u, v, z* are velocity component in the *x, y, z* direction. *Ax, Ay, Az* cross sectional area of the flow, ρ fluid density, *PSOR* the source term, v_f is the volume fraction of the fluid, and the Three-dimensional momentum equations given in the Eq 2 (Ghasemzadeh, 2013).

$$\frac{\partial u}{\partial t} + \frac{1}{v_f}\left(uA_x\frac{\partial u}{\partial x} + vA_y\frac{\partial u}{\partial y} + wA_z\frac{\partial u}{\partial z}\right) = -\frac{1}{\rho}\frac{\partial P}{\partial x} + G_x + f_x$$
$$\frac{\partial v}{\partial t} + \frac{1}{v_f}\left(uA_x\frac{\partial v}{\partial x} + vA_y\frac{\partial v}{\partial y} + wA_z\frac{\partial v}{\partial z}\right) = -\frac{1}{\rho}\frac{\partial P}{\partial y} + G_y + f_y \quad (2)$$
$$\frac{\partial w}{\partial t} + \frac{1}{v_f}\left(uA_x\frac{\partial w}{\partial x} + vA_y\frac{\partial w}{\partial y} + wA_z\frac{\partial w}{\partial z}\right) = -\frac{1}{\rho}\frac{\partial P}{\partial y} + G_z + f_z$$

Where P is the fluid pressure, G_x, G_y, G_z are the accelerations created by body fluids, f_x, f_y, f_z, are the viscosity acceleration in three dimensions, and v_f is related to the volume of fluid, defined by the Eq 3. For the modeling of free surface profile, the VOF Technique based on the volume fraction of the computational cells has been used. Since the volume fraction F represents the amount of fluid in each cell, takes Value between 0 and 1, (Karami, 2020).

2.3 Numerical Simulation of Flow and Sediment on FLOW-3D

$$\frac{\partial F}{\partial t}+\frac{1}{v_f}\left[\frac{\partial}{\partial x}(FA_x u)+\frac{\partial}{\partial y}(FA_y v)+\frac{\partial}{\partial y}(FA_z w)\right]=0 \quad (3)$$

The FLOW-3D numerical model generates a three-dimensional network structure composed of rectangular cube cells for the desired field. To achieve this, a three-dimensional model matching the specifications of the laboratory setup was first created using AutoCAD software. The results were then imported into FLOW-3D to generate a network and set boundaries using the tools FAVOR and VOF. After entering the geometric data into the software environment and defining the boundaries of the main and subsidiary canals, the target area was meshed using the VOF and FAVOR methods.

The optimal dimensions of the network were selected based on the required accuracy and computational time, and the field network was set up with orthogonal lines. For calculations in this study, two meshes were used, perpendicular to each other. One mesh was for the main canal, with dimensions of 1.8 m in length, 1.6 m in width, and 0.5 m in height. The other mesh was used for the intake, with dimensions of 0.7 m in length, 1.05 m in width, and 0.25 m in height. In total, 1,623,750 cells, each with dimensions of 0.01 m, were used to mesh the model. The RNG turbulence model was employed in the numerical modeling. After creating the computational network, boundary conditions, and initial conditions, simulations of flow and sediment transport were performed.

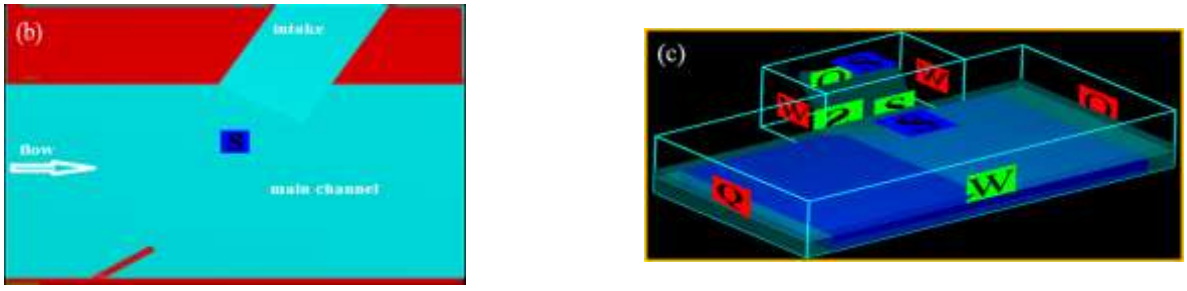

Fig. 2 a) laboratory model geometry together with the initial conditions, b) Model reticulation, and c) boundary conditions in the model (the main channel and intake).

2.4 Geometry, Meshing and the Model Boundary Condition

The main canal model was created in AutoCAD software and was recalled in export STL format in FLOW-3D environment. To reduce computing time in numerical simulations, a part of the experimental channel is usually considered (Fig. 2). Networking the model for a condition in which there is no structural model is shown in Figure 4. Figure 5 shows the model boundary conditions. The boundary condition of the flow inlet in the main canal flow (volume flow rate) is the entry height (fluid elevation), which was obtained through the experiments. In the inlet boundary condition, the sediment concentration entering the canal is also taken into account. The outlet boundary condition in the main canal was selected as outflow. The right wall of the main canal (against the intake) and the main canal floor were decided to be walls and the left wall (in fact on the side of the intake and the stream) was decided to be of symmetrical kind. Mesh boundary conditions for the intake was in a way that the inlet and water level were of symmetrical kind. The walls on its both sides and the floor were chosen to be walls and the flow outlet was chosen to be of outflow sort.

2.5 Calibrate the model

Due to the complex three-dimensional flow in the intake, the model must be calibrated to match laboratory conditions before simulation. In FLOW-3D, it was necessary to verify the Manning coefficient and the resulting roughness height. Therefore, this research involved calibrating the FLOW-3D numerical model by accurately estimating the Manning coefficient parameter, followed by calculating and estimating the roughness height. Calibration was conducted by comparing numerical and experimental results in two dimensions. For this purpose, the particle diameter (D50) was extracted from the grain size curve used in the experimental model. The Manning coefficient was then estimated at 0.014 using Subramanya's

relationship (1982). Finally, the roughness equivalent height was estimated using the Strickler and Johnson equation as 0.0025 and was introduced into the model. The results of the numerical simulation were compared with experimental results obtained in front of the intake in the main channel. In this study, the flow channel dimensions and mesh network were used for calibration based on the study's objectives. For calibration, three network configurations were considered (1, 2, and 5), and the results were compared with laboratory data. According to the calculation of the correlation coefficient and root mean square error (RMSE), as shown in Table 1 and Fig. 3, the highest correlation coefficient was approximately 0.91 for non-structured scenarios and 0.90 for structured scenarios. The lowest errors were 0.017 and 0.018, respectively, in other states. During the calibration step, the difference between laboratory and numerical data was compared. To evaluate the model against experimental results, both correlation and RMSE were used.

Table 1 Correlation coefficient and error in the calibration stage of the model

With the structure						No Structures						states Coefficients
Transverse speed Network number			Longitudinal speed Network number			Transverse speed Network number			Longitudinal speed Network number			
1	2	5	1	2	5	1	2	5	1	2	5	Network
0.87	0.90	0.86	0.90	0.94	0.89	0.87	0.89	0.88	0.90	0.91	0.88	R^2
0.020	0.018	0.021	0.018	0.016	0.020	0.019	0.017	0.018	0.014	0.012	0.015	RMSE

Fig. 3 Calibration of the model by the number of network changes, without structure, a) longitudinal velocity, b) transverse velocity. with structure, c) longitudinal velocity, and d) transverse velocity.

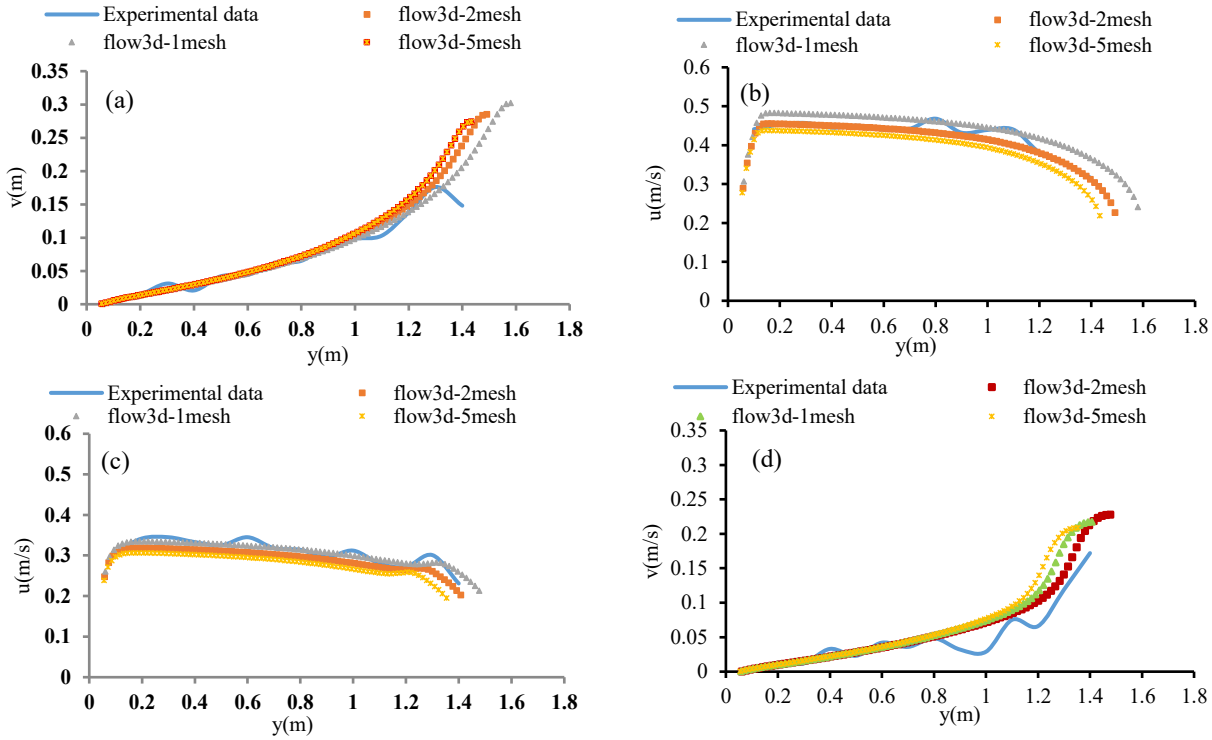

To ensure the model results, the model data and the experimental data were compared. According to the objectives of the present study, the size of the flow canal and sediment parameters were used for calibration. By changing the sediment parameters and mesh dimensions in the mathematical model, velocities in both longitudinal and transverse dimensions were compared in two sections of the canal width. One of the sections was in front of the mouth, upstream, at the junction of the upstream wall and the main canal (x=1.1), and the other one was downstream of the intake, at the junction of the downstream wall and the main canal (x=1.8). At 15 points of the path, velocity parameters were taken in two dimensions and in two sections (1.1 and 1.8). Then, according to Figs. 4 and 5, the model results were compared with the experimental results. The results of the velocity profiles in the main channel in the flow direction (u) and perpendicular to the flow direction (v) were taken and modeled, showing that there is a good overlap and acceptable agreement between the mathematical and experimental models. In the validation stage, the difference between the experimental and numerical data was compared. To evaluate the model results with the experimental results, the correlation coefficient and the RMSE function, the root mean square error, were used (Eq. 4).

Fig. 4 Calibrated velocity in the main channel (X=1.1), while no structures, a) longitudinal, b) transverse velocity. with structures, c) longitudinal velocity, and d) transverse velocity.

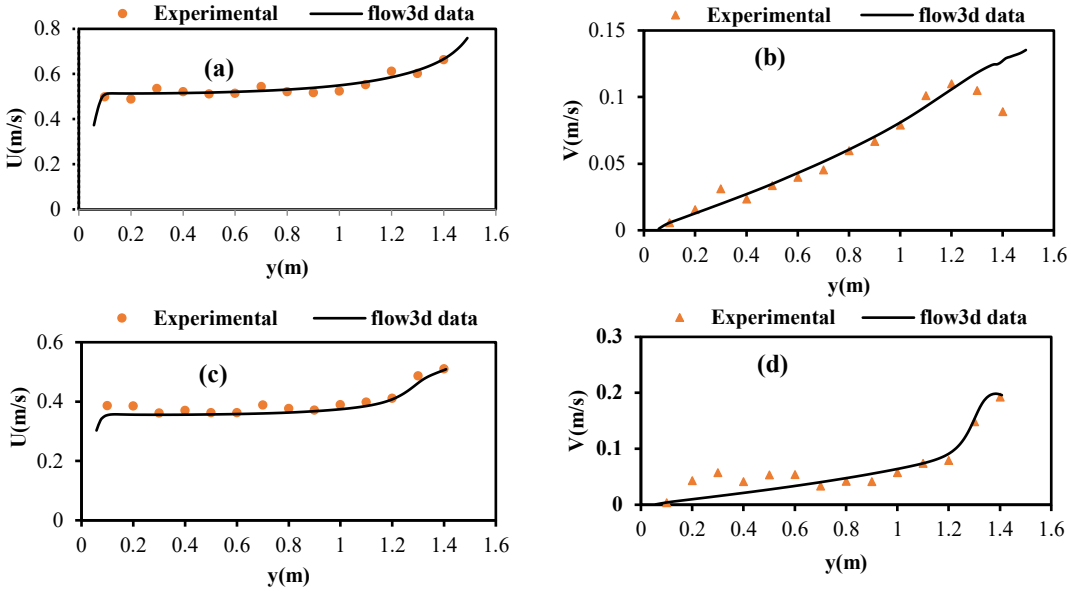

Fig. 5 Calibrated velocity in the main channel (x=1.8), while no structures, a) longitudinal, b) transverse velocity. with structures, c) longitudinal velocity, and d) transverse velocity.

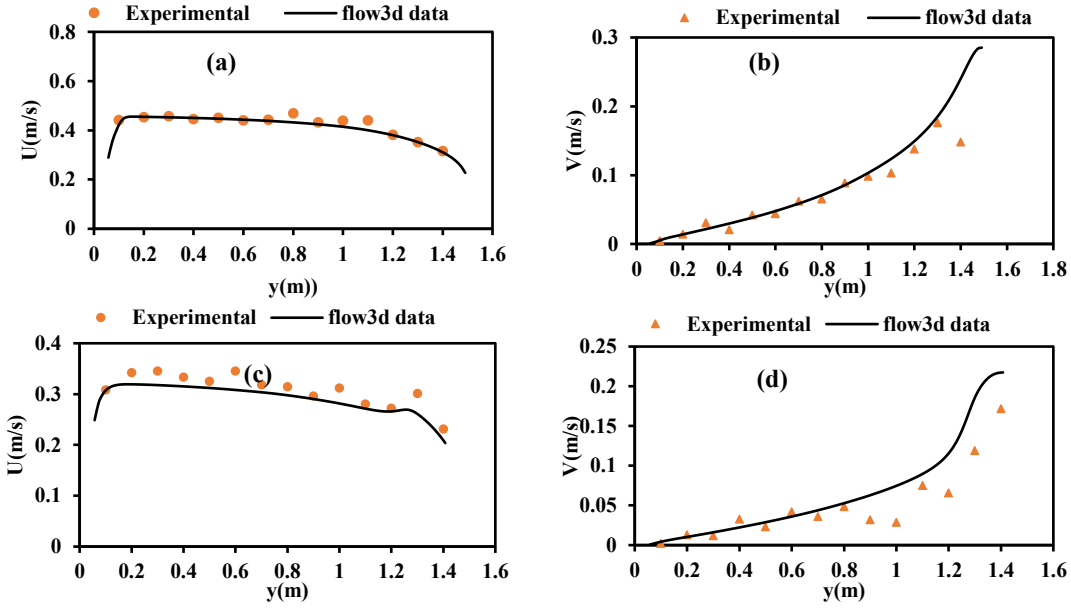

$$RMSE = \sqrt{\frac{\sum(Vo-Vc)^2}{n}} \quad (4)$$

where n is the number of data. V_o velocity measured in the laboratory; and V_c is the velocity obtained from the mathematical model (FLOW-3D). The values of the correlation coefficient and RMSE error, in the calibration and validation stages, are given in Table 2.

3. Results and Discussion

3.1 Without structure Condition

According to Fig. 6(a, b), the flow lines in the surface and near the canal bed were numerically drawn. By comparing the flow lines at different levels, it can be seen that the flow division line at the levels near the bed is broader than the higher levels in the main canal, moreover, the size of the separation zone within the intake is in such a way that at levels close to the bed, it is narrower than the higher levels and this causes a greater level of particles of the lower levels to be swept and guided into the intake. In the intake, the greatest amount of current passes along the right wall because in this area, the flow turns sharply. The flow rate is increased in the upstream of the intake canal, causing scour in the upper part. Inside the intake, the surface flow lines tend to the right wall and the bottom flow lines tend to the left wall (Fig. 6a-f).

Table 2 Correlation coefficient rate and the error in the calibration

Condition	Position	Coefficients	V	U (m/s)
No-structure	1.1=x	R^2	0.92	0.89
		RMSE	0.012	0.017
	1.8=x	R^2	0.91	0.90
		RMSE	0.025	0.016
With structure	1.1=x	R^2	0.90	0.94
		RMSE	0.018	0.016
	1.8=x	R^2	0.91	0.85

The dimensions of the separation zone on the surface of the intake's canal are more than those of its bottom. Due to the reduction of flow velocity in the separation zone and the reduction of the bed shear stress, there is sedimentation inside the intake canal. There is a vortex area inside the canal where the rotation direction of the vortex is clockwise. Inside the intake canal, there is an area where the maximum of flow constriction can be seen. In this area, the velocity increases as the flow is constricted. On arrival of the flow into the intake, due to its high velocity and hitting the wall it moves downstream towards the substrates. Of the intersection of this downward flow and the longitudinal flow inside the canal, a spiral flow is shaped in the intake, which moves in the direction of the flow towards the end of the intake, and it disappears after a short distance due to friction with the wall. In the intake inlet and in the vicinity of the upper wall of the canal (left side), another vortex area is created where the effective width of the inlet is reduced. There is sedimentation in this area. In the main canal below the intake inlet, a slight twisting flow is created and moving downwards, its intensity decreases, and it finally disappears. Compared to the surface, in the bottom layers of the flow inlet into the intake, the flowing lines have a smaller angle, which reduces the extent of the flow separation zone in the intake canal.

Fig. 6 Flow lines in two deep sections in the main canal and intake, without structure: a) On the surface, b) close to the bed. with skimming wall, c) On the surface, d) close to the bed. with a skimming wall and spur dike. e) On the surface and f) close to the bed

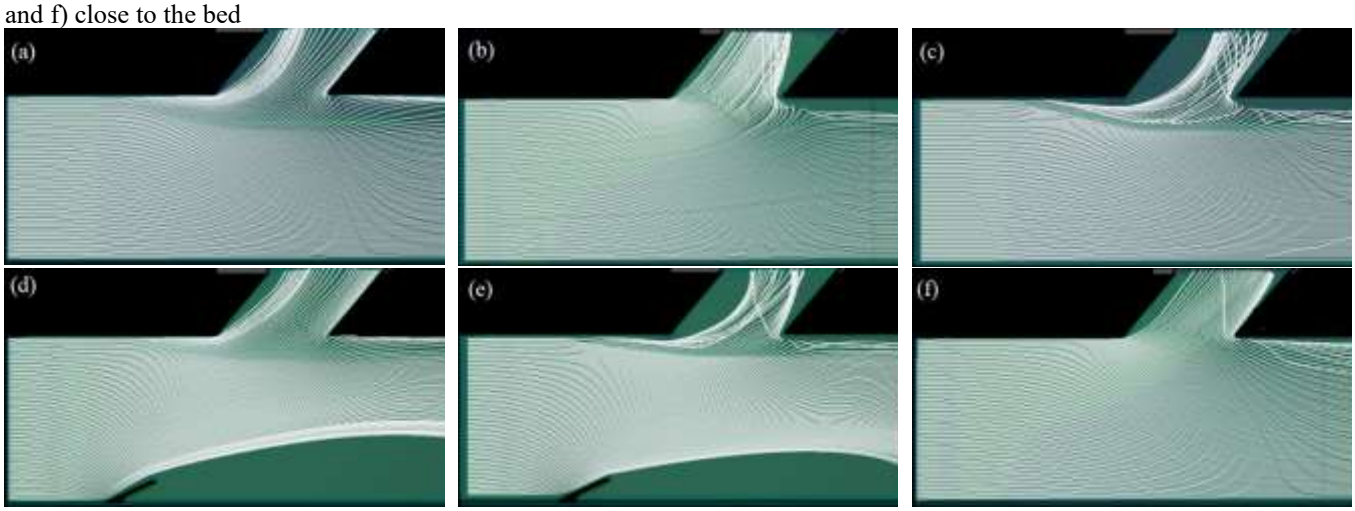

Fig. 7 Distribution of the velocity vectors in the plane (X-Y) in two depths: a) at the surface, b) near the floor

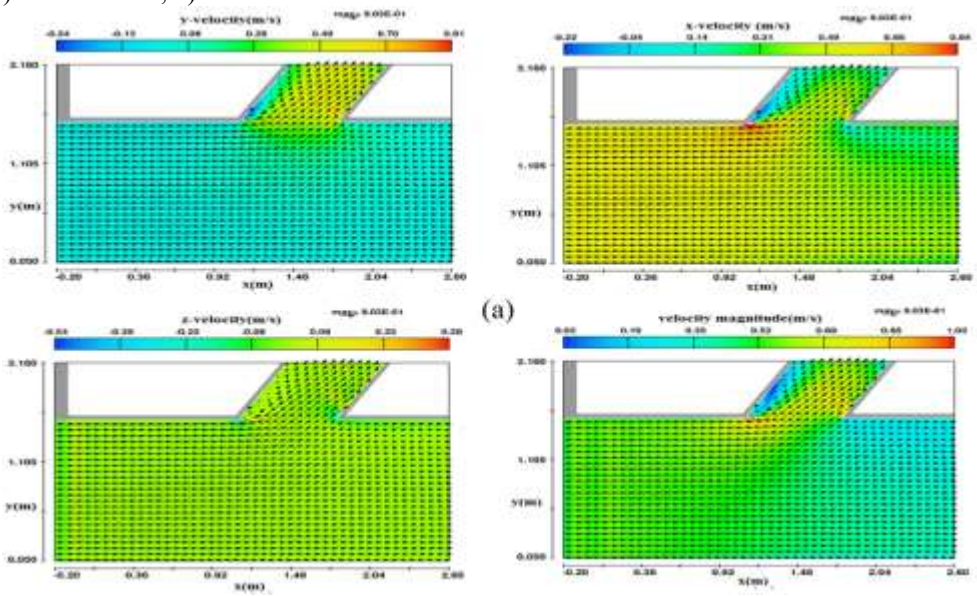

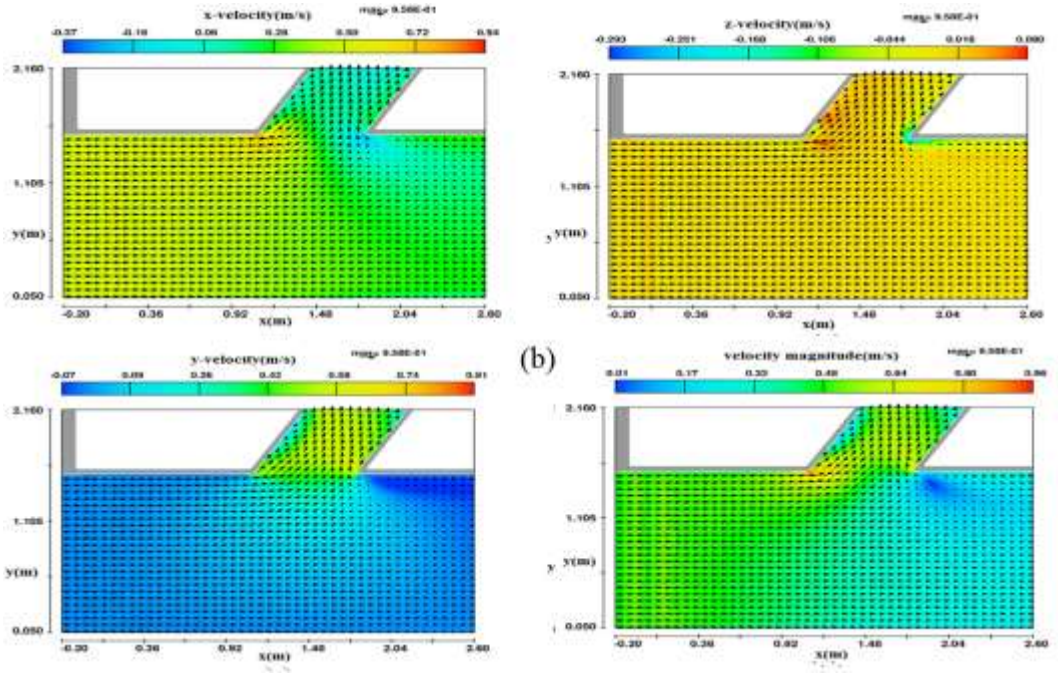

Figs. 7 and 8 show the equal amount of velocity and velocity vectors in the no-structure condition. The size of the velocity vectors has changed in different sections and situations. Counters and velocity vectors have been drawn on the page (x-y) for both surface and deep sections close to the bed. According to the figure, the maximum longitudinal velocity and the maximum total velocity have occurred at the beginning of the intake in its left corner. The maximum transverse velocity has occurred on the right side of the intake. In these figures, there are areas with secondary vortex flow downstream and on the left of the intake. Fig. 8 on page (x-z) shows the velocity longitudinal profile in three directions: length, width, and depth, and their resultant at a transverse distance of 27 cm from the intake inlet. According to the figure, we can see the maximum longitudinal velocity in the intake upstream; the maximum transverse velocity in the intake inlet; the maximum depth velocity in the canal upstream; and the maximum resultant velocity both in the intake inlet and upstream.

3.2 With Skimming Wall Structure Condition

By installing the skimming wall in front of the intake, the bed profile in the intake front and the flow pattern changes, and the vortex area moves. The skimming wall prevents bedload from entering and large sediment accumulation in the intake and enhances the efficiency. The flow velocity near the bottom layer of the intake increases. Dimensions of the stationary area in front of the intake, the inlet of which is on the left side, are reduced compared to the no-structure condition. Given that the lower flow layers have more sediments than the upper layers, by installing the skimming wall in front of the intake, a large amount of sediments entering it is removed and guided downstream the main canal. The size of the velocity vector angle towards the intake decreases in the bottom layers. This is due to the swirling flow caused by the skimming wall.

Fig. 8 Velocity distribution in the main channel and page (X-Z)

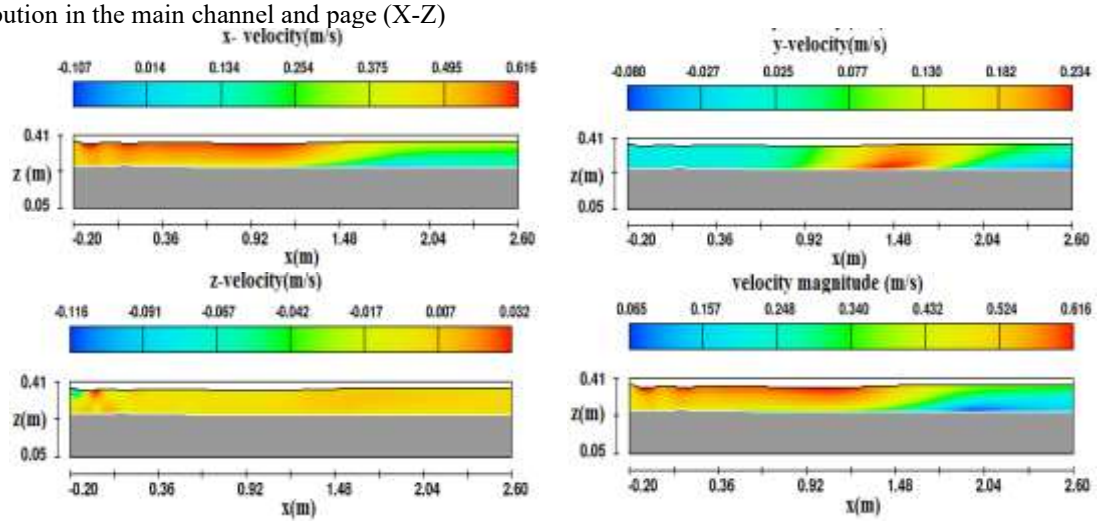

Fig. 9 Distribution of the velocity vectors in the plane (X-Y) in two depths: a) at the surface and b) near the floor

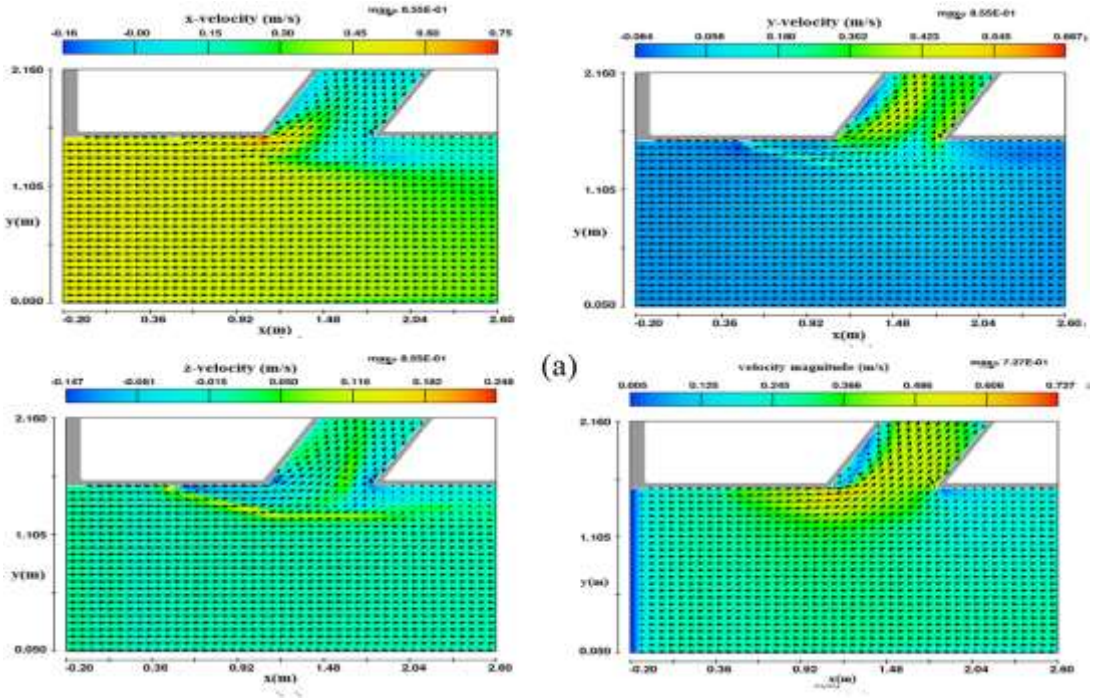

a) at the surface and

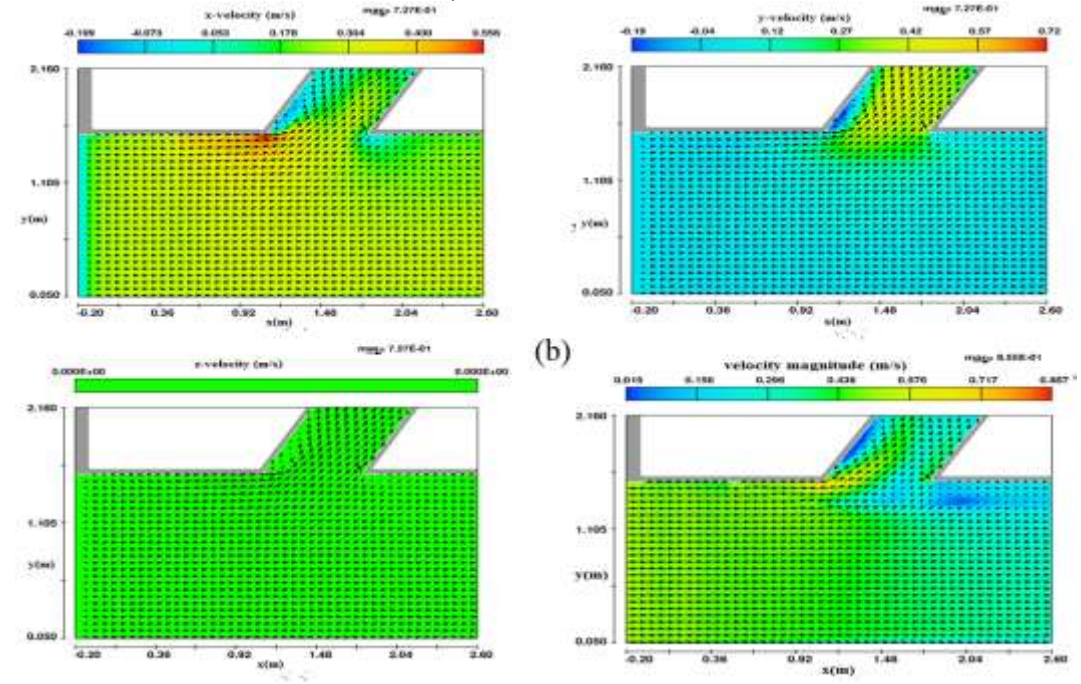

b) near the floor

Figs. 9 to 10 indicate the equal amount of velocity and velocity vectors in the presence of a skimming wall. The size of the velocity vectors has changed in different sections and situations. Counter and velocity vectors have been drawn on the page (x-y) for both surface and deep sections close to the bed. According to the figure, the maximum longitudinal velocity and the maximum total resultant velocity have occurred at the beginning of the intake in its left corner. The maximum transverse velocity has occurred on the right side of the intake. In these figures, there are areas with secondary vortex flow downstream and on the left of the intake. Fig. 10 on page (x-z) shows the velocity longitudinal profile in three directions: length, width, and depth, and their resultant at a transverse distance of 27 cm from the intake inlet. According to the figure, we can see the maximum longitudinal velocity in the intake upstream; the maximum transverse velocity in the intake inlet; the maximum depth velocity in the intake inlet; and the maximum resultant velocity both in the intake inlet and upstream.

Fig. 10 Velocity distribution in the main channel and page (X-Z)

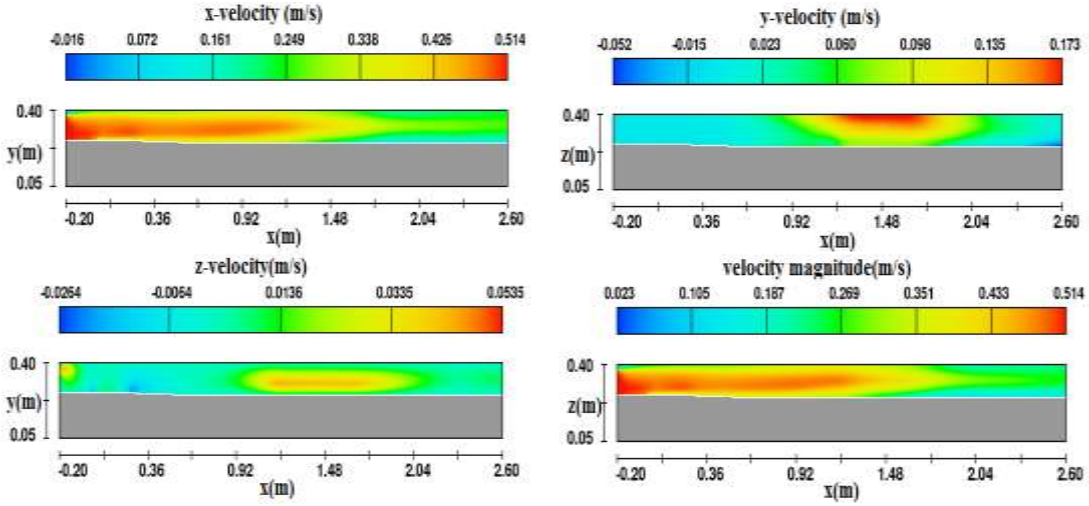

3.3 Using Skimming Wall and Spur Dike on the Opposite Side

By installing a spur dike, the flow velocity is increased in front of the intake and decreased behind the spur dike, and swirling flow is created. The slowdown in alluvial beds causes sediment accumulation behind the spur dike. Due to the spur dike effects in the main canal, after passing through the intake, the flow direction is more intense and opposite to the intake. By installing the spur dike, the flow pattern changes, and flow lines in the upper layers continue uniformly and parallel to the downstream in the main canal (Fig. 11a and b). In the main canal and in front of the intake, a secondary stream that was created after the intake almost disappears as the flow velocity increases. The flow separation plane on the floor is influenced by the construction of the spur dike. Using a combination of the skimming wall and the spur dike on the opposite sides, the flow velocity is increased in front of the intake compared to the previous states. The spur dike leads the flow towards the intake, passes it at a high velocity in front of the intake, thus washing the sediments and carrying them downstream. And a groove is created in front of the intake, which causes sediments to move down and away from it. As shown in Fig. 11 a and b, the spur dike guides the surface layers with less sediment towards the intake and the substrates that carry more sediment away from the intake. The spur dike creates a transverse flow. This flow is combined with the swirling flow created by the skimming wall and increases the inflow to the intake.

Fig. 11 Distribution of the velocity vectors in the plane (X-Y) in two depths: a) at the surface and b) near the floor

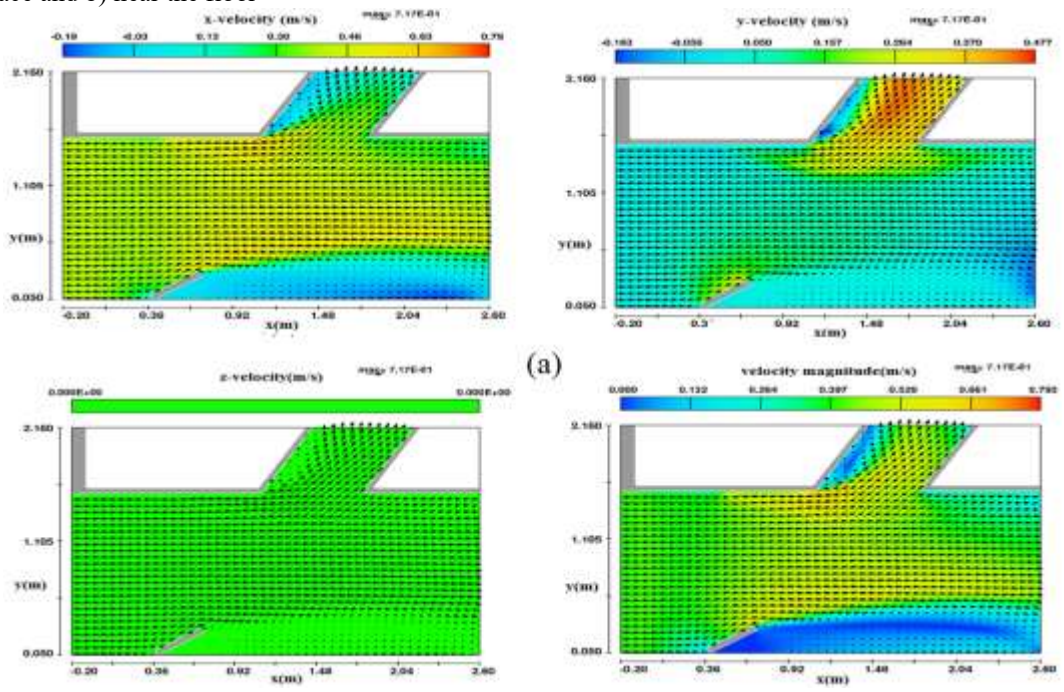

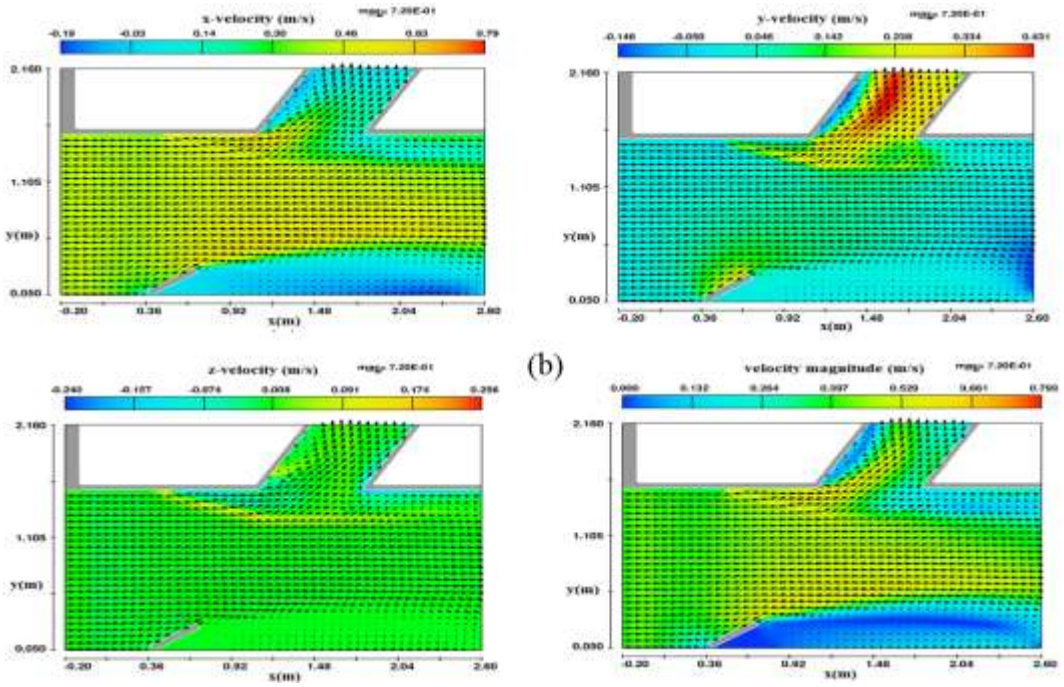

Figs. 11 and 12 show the values of flow lines and velocity counters in the transverse and longitudinal sections. Fig. 11 shows the velocity vectors within the skimming wall and the spur dike. In this figure, the vortex flows formed around the spur dike cape, the turbulence, and the separation zone are clearly indicated. The maximum longitudinal velocity happens around the spur dike cape, and it causes scouring in the area. Having passed through the spur dike, the maximum velocity gradually moves to the middle of the canal and towards the outer wall. Downstream of the spur dike in the vicinity of the spur dike's adjacent wall, a calm zone is formed due to low velocity caused by the formation of the vortex: Sedimentation occurs in this area. As can be seen in Fig. 11, in the spur dike downstream, we can see negative longitudinal velocities and it indicate the presence of counterclockwise vortexes there. It also reveals the spur dike's effects in creating a low velocity zone adjacent to the bank and in leading the flow towards the opposite bank.

In Fig. 12, the counters and velocity vectors have been drawn on the page (x-y) for both surface and deep sections close to the bed. According to the figure, the maximum longitudinal velocity and the maximum resultant velocity have occurred at the beginning of the intake in its left corner. The maximum transverse velocity has occurred in the central part of the intake. In these figures, there are areas with secondary vortex flow downstream and on the left of the intake. The Fig. 12 on page (x-z) shows the velocity longitudinal profile in three directions, length, width, and depth, and their resultant at a transverse distance of 27 cm from the intake inlet. According to the figure, we can see the maximum longitudinal velocity in the intake upstream; the maximum transverse velocity in front of the intake inlet; the maximum depth velocity in front of the intake inlet; and the maximum resultant velocity both in the intake inlet and upstream.

Fig. 12 Velocity distribution in the main channel and page (X-Z)

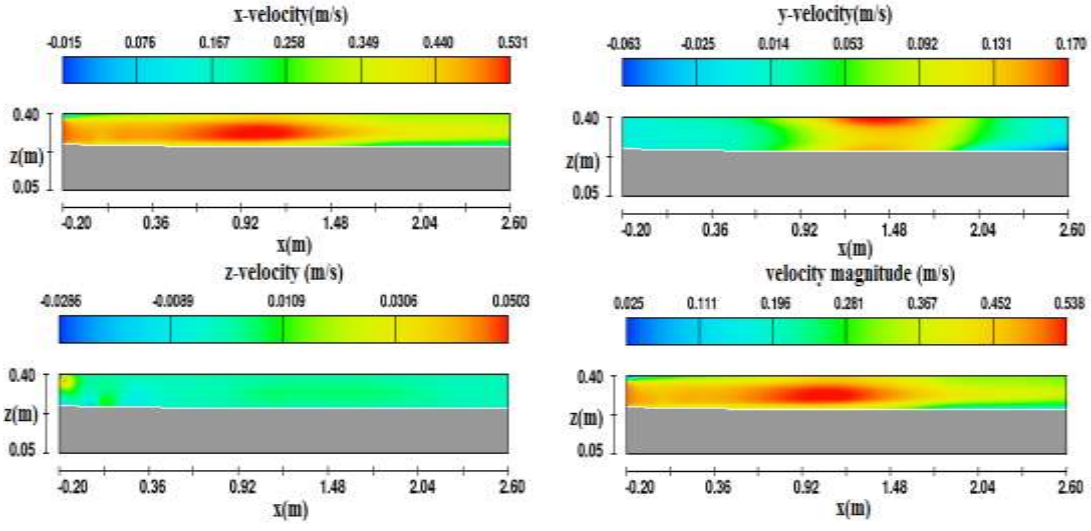

The findings of this research were compared with the studies conducted by Moradinejad et al. (2019), Tabrizi et al. (2019), and Goleij et al. (2019). It was concluded that the results align with these studies. Moradinejad et al. (2019) concluded in their research that the width of the narrowing area of flow in the intake decreases from the channel floor to the water surface. In this narrowing area, the flow depth is minimized and approaches the critical depth. Despite the presence of secondary currents within the intake, sediment entering the intake moves toward the separation zone and subsequently downstream. By installing a spur dike at the intake, the width of the separation zone is reduced near the channel bottom but increases at the water surface. As a result, the area affected by the intake on the channel bottom decreases, while the amount of sediment entering the intake is also reduced. Tabrizi et al. (2019) demonstrated that under experimental conditions, the flow dividing line at upper levels of the flow shifts away from the outer wall of the main channel. Conversely, at lower levels of flow—where sediment concentration is higher—it approaches this wall. In other words, more water intake occurs at upper levels with less sediment content. Their analysis of transverse velocity component diagrams revealed that increasing the water intake ratio (compared to conditions without a spur dike structure) significantly reduces the dimensions of the flow separation zone formed in the diversion channel (intake). Consequently, both its length and width reach minimum values. Goleij et al. (2019), in their study examining flow separation width at both the water surface and near-bed levels in a U-shaped main channel, found that the dewatering ratio was the most critical factor influencing this hydraulic parameter. At the water surface, an increase in dewatering percentage led to an increase in flow separation width. The use of skimming wall structures with a 12-degree angle at the intake further increased flow separation width due to vortex formation and enhanced surface flow conduction. However, near-bed levels showed different behavior: in control experiments and those with sills, flow separation width increased with higher dewatering percentages. When skimming wall structures (angled at 12 degrees) were combined with a sill, this parameter decreased near-bed levels as dewatering percentage increased. Additionally, incorporating a spur dike alongside these two structures further reduced the near-bed flow separation width.

4. Conclusion

In this study, a skimming wall structure has been used for the first time to control sediment in front of a lateral intake. This structure changes the flow pattern around the lateral intake opening. Therefore, the aim of this study is to solve the three-dimensional flow field around a lateral intake located in a straight path using the FLOW3D numerical model and compare it with a laboratory model. In the laboratory, experiments were conducted on the flume and the results were compared with the numerical model. The results of the study are as follows.

1. The results showed that in the absence of a structure, inside the main channel, the flow separation width at levels near the bed is wider than at higher levels.

2. By installing a skimming wall in front of the intake, the flow separation width near the bed, which has more sediment, decreases and increases at the level with less sediment, causing less sediment to enter the intake.

3. Inside the intake, the surface flow lines tend towards the right wall, and the flow lines of the lower layers tend towards the left wall of the intake. The width of the flow separation area at the surface is greater than at the bottom.

4. Also, the presence of the spur dike has caused the longitudinal velocity in the near-bottom layer to increase by 2.25 times and the transverse velocity in the surface layer to increase by 1.33 times compared to the case without spur dike.

Considering the novelty of the combination of the skimming wall and spur dike, the lack of use of different landings and spur dike with different dimensions and positions is one of the limitations of this research.

It is suggested that the present research be conducted with different Froud number and the effect of the Froud number on sediment control, and also using other mathematical models such as SSIM and CCHEE2 to simulate flow and sediment, and compare it with this research.

Statements and Declarations

Data availability

The data used in this research are presented in the text of the article.

Conflicts of interest

The author of this paper declared no conflict of interest regarding the authorship or publication of this paper.

Author contribution

A. Moradinejad: Data Collection, Modeling and Results Analysis; A. Haghiabi; Results Analysis and Research Management; M. Saneie: Research Management; H. Younesi: Results Analysis.

AI Use Declaration

This study did not incorporate artificial intelligence techniques; instead, all analyses and optimizations were conducted using conventional and widely accepted analytical methods.

References

Abbaspour, A., Farsadizadeh, D., Hosseinzadeh Dalir, A., & Sadraddini, A. A. (2009). Numerical study of hydraulic jumps on corrugated beds using turbulence models. *Turkish Journal of Engineering and Environmental Sciences 33(1):61-72*. https://doi.org/10.3906/muh-0901-7

Acharya, A., & Duan, J. G. (2013). Three dimensional simulation of flow field around series of spur dikes. International Refereed *Journal of Engineering and Science, 2(7), 36-57.* https://doi.org/10.1061/41173(414)218

Aghaei Daneshvar, F., & Taleb Beidokhti, N. (2015). Numerical simulation of turbulent flow bed scour around a spur dike with numerical models. *Journal 10*(1), *Spring.*

Ahmed, K. O., Kavianpour, M. R., Amini, A., & Aminpour, Y. (2025). Numerical assessments of scour depth

predictions downstream of box culverts under various flow and blockage conditions. *Discover Applied Sciences*, 7(3), 211. DOI: https://doi.org/10.1007/s42452-024-06391-2

Amini, A., Arya, A., Eghbalzadeh, A., & Javan, M. (2017). Peak flood estimation under overtopping and piping conditions at Vahdat Dam, Kurdistan Iran. Arabian Journal of Geosciences, 10(6), 127. https://doi.org/10.1007/s12517-017-2854-y

Amini, A., Mohammad Ali, T., & Ghazali. A.H. (2024). Optimizing and Evaluation of Scour Depth Prediction Methods for Columns as A Component of Complex Bridge Piers. *Adv. Civil Eng. Environ. Sci., 2024, 1(1)*. https://doi.org/10.22034/ACEES.2024.477822.1008.

Amirarsalani, S. H. (2008). Numerical investigation of free falling jet's effect on the scour of plunge pool. XVIII International conference on water resources. (In Persian).

Ardeshir, M., Sanei, M., & Rezaei, Z. (2014). Effect of length and Spur dike permeable and non- submerged abutment on changes in discharge angle of 90 degrees. Ninth International Seminar of River Engineering in Ahvaz, Iran. (In Persian).

Ettema, R. & Muste, M. (2004). Scale effects in flume experiments on flow around a spur dike in flatbed channel. *J. Hydr. Engin. 130: 635-646.* DOI:10.1061/(ASCE)0733-9429(2004)130:7(635)

Ghasemzadeh, F. 2013. 2nd edition 2013. Simulation of hydraulic problems in FLOW 3D.

Goleij, H., Haghiabi, A. H., Saneie, M., & Hojattallah Yonesi, H. (2019). Investigation dimensions of separation zone at lateral intake and flow pattern in a U channel bend with presence sill, dike and skimming wall. *Watershed Engineering and Management Volume 11, Issue 1*, https://doi.org/10.22092/ijwmse.2017.115351.1355.

Hsu, C., Tang, C., Lee, W. & Shieh, M. (2002). Subcritical 90 equal-width open-channel dividing flow, *Journal Of Hydraulic Engineering, Vol. 128, No.7, , pp.716-720*. DOI: 10.1061/(ASCE)0733-9429(2002)128:7(716)

Karami Moghadam, M., Amini, A., & Keshavarzi, A. (2020). Intake design attributes and submerged vanes effects on sedimentation and shear stress. *Water and Environment Journal*. https://doi.org/10.1111/wej.12471

Karimi Sarmeydani, I., Heidarnejad, M., & Egdernezhad, A. (2024) Quantitative Simulation of iverged Flow Using Machine Learning Techniques and FLOW-3D Numerical Modeling. *Irrigation and Drainage Structures Engineering Research/Vol.25/No.96 Autumn /2024/P: 27-46.* https://doi.org/10.22092/idser.2024.366862.1591

Li, C. W., & Zeng, C. (2009). 3D numerical modeling of flow divisions at open channel junctions with or without vegetation. *Advances in Water Resources, 32(1), 49-60.* https://doi.org/10.1016/j.advwatres.2008.09.005.

Moradinejad, A., Haghiabi, A., Saneie, M., & Yoneseie, H. (2017). Investigating the effect of skimming wall on controlling the sediment entrance at lateral intakes. *Journal of Water Science & Technology: Water Supply. (IWA Publishing). 17.4* .DOI: 10.2166/ws.2017.007

Moradinejad, A., Sanei, M., Ghaderi, A., & Mahyar Zamanieh Shahri, S. (2019). Experimental study of flow pattern and sediment behavior near the intake structures using the spur dike and skimming wall. *Applied Water Science 9:195*. https://doi.org/10.1007/s13201-019-1069-7

Neary, V. S., Sotiropoulos, F., & Odgaard, A. J. (1999). Three-dimensional numerical model of lateral-intake inflows. *Journal of Hydraulic Engineering, 125(2), 126-140.* https://doi.org/10.1061/(ASCE)0733-9429(1999)125:2(126)

Pour Bahman, P. (2015). Flow Simulation sediment pumping station intake structure Flow3d. Eleventh Iranian Hydraulic Conference.

Rahmani Firuzjany, M., Salehi Nishapur, A. A., & Ehsan, M. (2015). Simulated the effect of the angle of the intake flow pattern in the lateral intakes using the software FLOW-3D. Tenth International River Engineering Seminar 92 January to 1 Persian date Bahman, Ahwaz Chamran University [In Persian].

Sarvari, M., Tkldany Amiri, A. & Rostami, M. (2015). Evaluation of FLOW-3D Numerical Model in Predicting the Morphological Changes at River Junction. *Journal of Hydraulics, 10(1),* 53-63. 10.30482/jhyd.2015.11818

Shahrokhy, M. (2008). Comparison of turbulence models on turbulent flow. 4th Congress of Civil Engineering. Tehran University.

Shamlou, H., & Jaffari, P. (2008). Numerical investigation of effect of bottom roughness on flow around the piers by Flow3D. 4th Congress of Civil Engineering. Tehran University.

Subramanya, K. (1982). Flow in open channels. Tata McGraw-Hill Publishing Company Limited.

Tabrizi, H., Haghiabi, A. H., Saneie, M., & Hojattallah Yonesi, H. (2019). Evaluation of spur dike effect on sediment and flow hydraulic of side intakes located on channel bends. *Watershed Engineering and Management Volume 9, Issue 3, Pages 346-359. (In Persian).*https://doi.org/10.22092/ijwmse.2017.109832.1281

Zhou, J., & Zeng, C. (2009). 3-D hybrid LES-RANS model for simulation of open-channel T-diversion flows. *Water Science and Engineering, 2009, 2(3): 13-26.* https://doi.org/10.3882/j.issn.1674-2370.2009.03.002